19th International Conference
ENGINEERING MECHANICS 2013
Svratka, Czech Republic, May 13 – 16, 2013

SPAN-WISE DISTRIBUTION OF LOSSES IN PRISMATIC TURBINE CASCADE

J. Fürst[1], M. Luxa[2], D. Šimurda[2]

Summary: *The paper deals with the experimental and numerical research of flows through prismatic turbine cascade in transonic regimes. The primary goal is to evaluate the influence of the non-uniformity of the inlet velocity profile to the span-wise distribution of energy losses. The numerical simulation with inlet velocity profile corresponding to the parameters of the flow in high speed wind tunnel in Nový Knín is compared to the experimental data. Next, the simulation assuming different inlet velocity profiles are used to evaluate the effect of the boundary layer in front of the cascade to the span-wise distribution of energy losses.*

1. Introduction

The flow through a turbine cascade is influenced by the interaction with end walls. The secondary flows comming from the development of the end-wall boundary layers cause an aditional losses which affects the overall performance of the turbine cascade. The problem of secondary flows is discussed in the literature, for a review see Lampart (2009a), Sieverding (1985). The complex flow structure of the secondary flows leads to non-trivial distribution of energy losses past the turbine blades. The pitch-averaged loss distribution posses usually local maxima at certain distance from the end-walls. Moreover, the non-uniformity of the flow field causes also the changes in the exit flow angle.

The effects of blade geometry and some flow parameters on the losses in subsonic axial turbines were investigated e.g. in Lampart (2009b). In the case of flows with supersonic exit velocities one has to account for the additional 3D effects originating form the interaction of the shock waves with the non-uniform flow field in the vicinity of end-walls.

Present contribution is focused on the secondary flow structure and the distribution of energy losses and flow angles in the transonic turbine blade cascade SE1050. The flow fields are calculated for different inlet velocity profiles and the effect of the inlet boundary layer thickness is discussed.

2. Test Blade Cascade

The turbine cascade SE1050 is a freely available test case for transonic flows in turbomachinery Kozel and Příhoda (2004), Šťastný and Šafařík (1990). The profile was designed for 1085 mm

[1] Doc. Ing. Jiří Fürst, PhD.: Fac. of Mech. Eng., Czech Technical University in Prague, Karlovo nám. 13; 121 35, Prague; CZ, e-mail: Jiri.Furst@fs.cvut.cz
[2] Ing. Martin Luxa, PhD., Ing. David Šimurda, PhD.: Institute of Thermomechanics AS CR, v. v. i., Dolejškova 1402/5, 182 00 Praha 8; CZ, e-mail: luxa@it.cas.cz

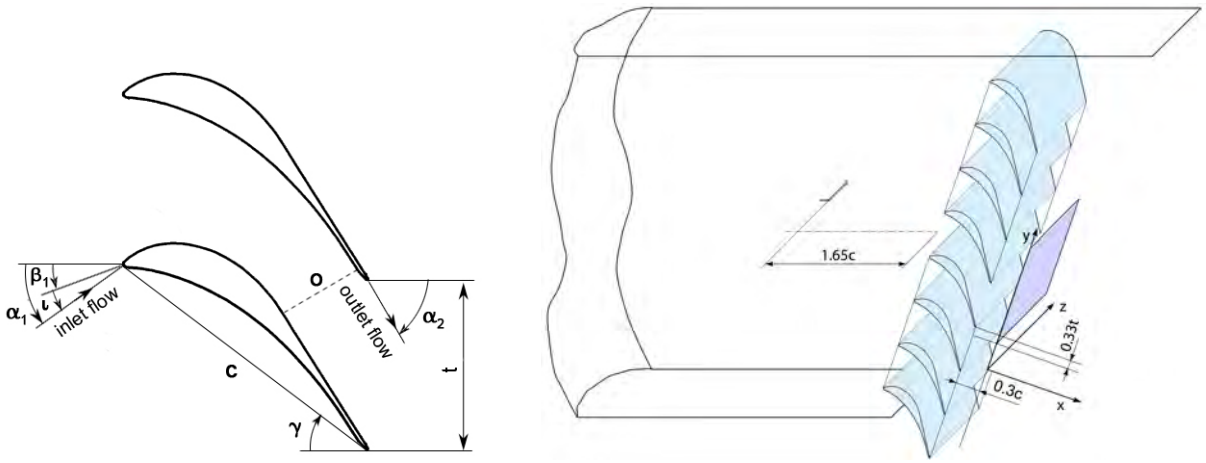

Figure 1: The scheme of the cascade (left), the sketch and the photo of the test cascade (right).

long rotor blade of the last turbine stage and it represents section located at the distance 320 mm from the root. Characteristic dimensions of the blade cascade model are apparent from Figure 1 and Table 1, respectively. Profile coordinates may be found in Kozel and Příhoda (2004).

Table 1: Geometry of the cascade.

Pitch	t	55.12 mm
Chord	c	100.0 mm
Throat	o	28.1 mm
Stagger Angle	γ	37.11 °
Inlet Metal Angle	β_1	19.3 °
Incidence	i	0.0 °
Blade length h	160.0	mm

All measuremetns were performed in the suction-type high-speed wind tunnel stationed in the Aerodynamic Laboratory of the Institute of Thermomechanics AS CR, v.v.i. in Nový Knín. During measurements, the tested blade cascade was fixed to sidewalls of a rotatable test section. Parameters of the inlet flow were measured by the Prandtl probe and three static pressure taps on the side-wall of the test section. Distributions of static pressure $p_2(z, y)$, total pressure $p_{t2}(z, y)$, pitch angle $\alpha_2(z, y)$ and yaw angle $\gamma_2(z, y)$ in the exit flow field were measured in the traversing plane located $0.3c$ behind the trailing edge plane. The traversed region covered two pitches and spanned over 140 mm of the 160 mm wide test section. For each of the two investigated regimes, measurements consisted of 17 pitchwise continuous traverses with 10 mm spanwise spacing in the center and 5 mm spacing at the edges of the traversing plane. Exit flow field distributions were measured using a traversing device with calibrated five-hole conical probe. The traversing device was equipped with PID controller, which utilizes pressure difference from the two vertically located pressure taps of the five-hole conical probe and sets the probe against the flow. The pitch angle was then measured by an angular transducer.

The accuracy of the measuring equipment enables us to measure the kinetic energy loss coefficient ζ with absolute uncertainty less than 0.4%, the pitch angle α_2 and the yaw angle γ_2 with absolute uncertainty less than $1°$. Periodicity of the exit flow field was assessed using so called "Sliding data reduction method", see Matějka et al. (2010). Distributon of loss coefficient ζ in the midsection evaluated by this method ranged within band of width 0.005 and analogical distribution of exit flow angle ranged in band of width $7°$. This aperiodicity in exit flow angle probably results from relatively low number of blades, see Luxa et al. (2012).

2.1. Inlet velocity profile

The inlet velocity profile have been formed thanks to the relatively very long inlet channel placed upstream the cascade.

The inlet velocity profile was obtained applying pneumatic measurement methods. The total pressure distribution across the channel $p_{1t} = f(z)$ was measured by a special shaped Pitot pressure probe, that is suitable also for measurement near the sidewall (see Fig. 2). The static pressures (p_{1s}, p_{2s}, and p_{3s}) were measured by three pressure taps situated on the sidewall in the vicinity of the position of Pitot probe. The arithmetic mean of these static pressure data was used for the velocity calculation:

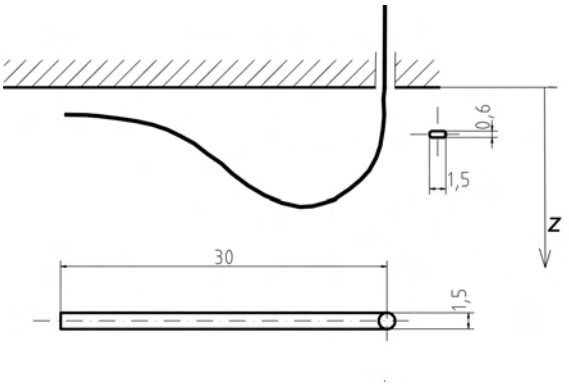

Figure 2: The Pitot probe

$$p_1 = \frac{p_{1s} + p_{2s} + p_{3s}}{3}. \qquad (1)$$

The inlet Mach number is then given by the relation:

$$M_1(z) = \sqrt{\frac{2}{\kappa - 1}\left[\left(\frac{p_{t1}(z)}{p_1(z)}\right)^{\frac{\kappa-1}{\kappa}} - 1\right]}. \qquad (2)$$

The evaluated Mach number $M_1(z)$ is shown in the Fig. 3 for different reference values of the inlet Mach numbers.

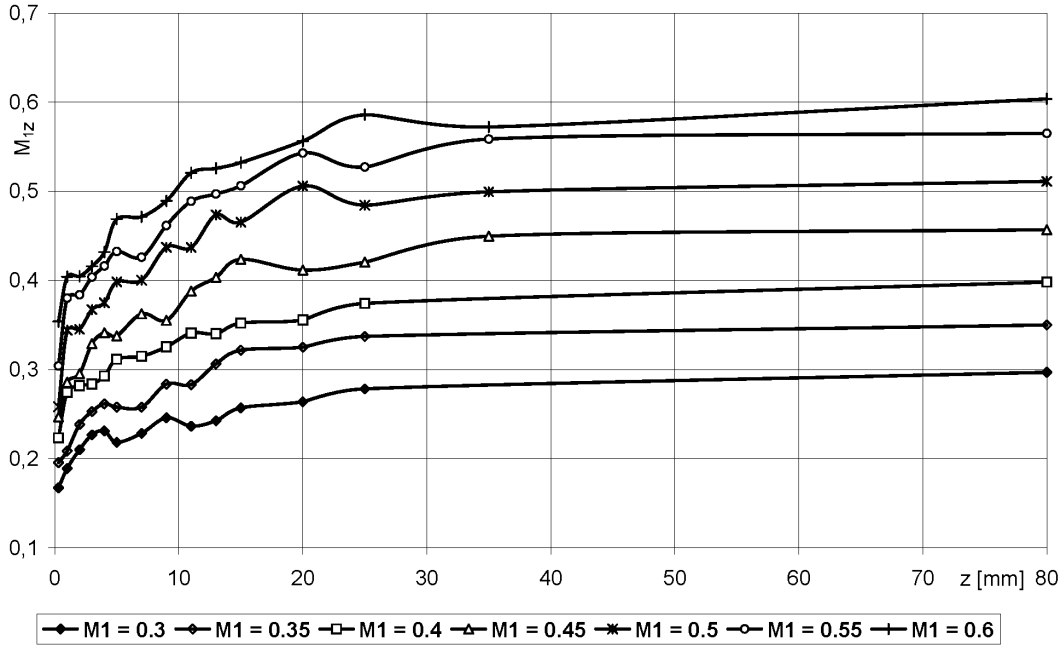

Figure 3: The distribution of inlet Mach number across the inlet channel.

3. Numerical simulations

The flow through the turbine cascade was modeled using the system of time-averaged Navier-Stokes equations for compressible flows, see eg. Ferziger and Peric (1999):

$$\frac{\partial \rho}{\partial t} + \frac{\partial(\rho u_j)}{\partial x_j} = 0, \tag{3}$$

$$\frac{\partial(\rho u_i)}{\partial t} + \frac{\partial(\rho u_i u_j)}{\partial x_j} + \frac{\partial p}{\partial x_i} = \frac{\partial(t_{ij} + \tau_{ij})}{\partial x_j}, \tag{4}$$

$$\frac{\partial(\rho E)}{\partial t} + \frac{\partial[(\rho E + p)u_j)}{\partial x_j} = \frac{\partial}{\partial x_j}\left[u_i(t_{ij} + \tau_{ij}) + \left(\frac{\mu}{Pr} + \rho\alpha_\theta\right)\frac{\partial h}{\partial x_j}\right], \tag{5}$$

where ρ is the density, u_i are the components of the velocity vector, p is the static pressure, E is the specific total energy, $h = E + p - u_i u_i/2$ is the specific enthalpy, t_{ij} is the viscous stress tensor, $\tau_{ij} = -\overline{\rho u_i' u_j'}$ is the Reynolds stress tensor, μ is the viscosity, Pr is the Prandtl number, and α_θ is the turbulent thermal diffusivity. The perfect gas (the air) with $p = (\kappa - 1)(\rho E - \rho u_i u_i/2)$ where $\kappa = 1.4$ is the constant specific heat ratio is assumed. The flow is Newtonian with constant viscosity μ, hence $t_{ij} = 2\mu(S_{ij} - \frac{1}{3}S_{ll}\delta_{ij})$ where $S_{ij} = (\partial u_i/\partial x_j + \partial u_j/\partial x_i)/2$. The Reynolds stress tensor is approximated using eddy viscosity approach

$$\tau_{ij} = 2\rho\nu_T(S_{ij} - \frac{1}{3}S_{ll}\delta_{ij}) - \frac{1}{3}\rho k\delta_{ij}, \tag{6}$$

where ν_T is the turbulent kinematic viscosity and k is the turbulent kinetic energy. The turbulent viscosity ν_T (or $\mu_T = \rho\nu_T$) and turbulent kinetic energy were calculated with the two-equation $k - \omega$ SST model, see Menter (1994).

The numerical solution was obtained with the finite volume method, namely with an in-house develped modification of `rhoSimpleFOAM` solver from freely available `OpenFOAM` package. The solver uses segregated approach (SIMPLE loop) and employs limited second-order interpolations. The results were compared to calculations performed with second independent in-house finite volume solver. The second solver uses AUSM fluxes with piece-wise linear reconstructions for convective terms, the central scheme for diffusive terms, and the implicit backward Euler method for time marching, see Fürst (2006).

The simulation was carried out assuming the periodicity in pitch-wise direction and symmetry in span-wise direction. The inlet plane was located 0.25c before the leading edge and the outlet plane was at axial distance 0.5c behind the trailing edge. The average static pressure corresponding to given regime with $M_{2i} = 1.198$ was prescribed at the outlet plane and two sets of boundary conditions were used at the inlet plane:

1. uniform inlet profile with constant total pressure $p_{1t} = 1 \times 10^5$ Pa, constant total temperature $T_{1t} = 293.15$ K, constant flow angles $\alpha_1 = 19.3°$, $\gamma_1 = 0°$, constant turbulence intensity $Tu = 2\%$ and turbulent frequency $\omega = 10\,400\,\mathrm{s}^{-1}$, and

2. inlet with non-uniform profile of total pressure with other quantities same as in the first case.

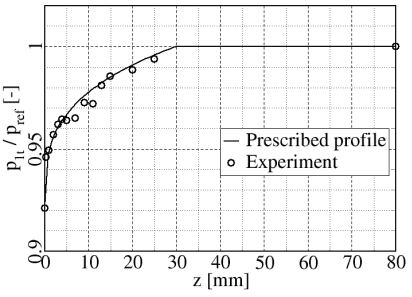

Figure 4: Measured and prescribed inlet profiles of the total pressure p_{1t}.

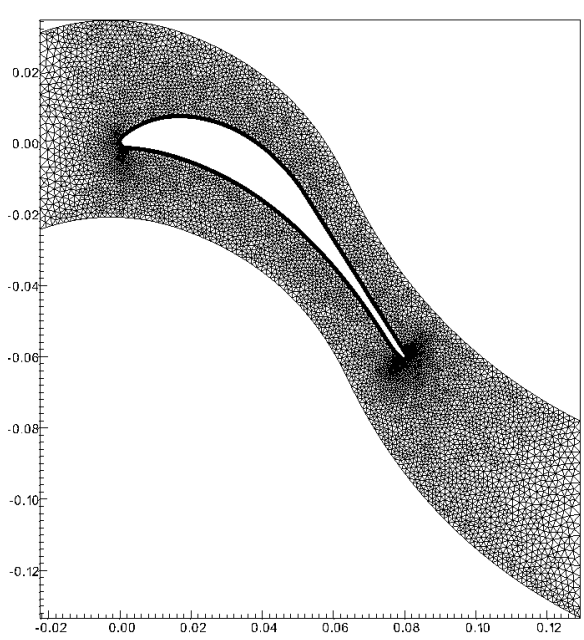

(a) Unstructured mesh (mesh 1)

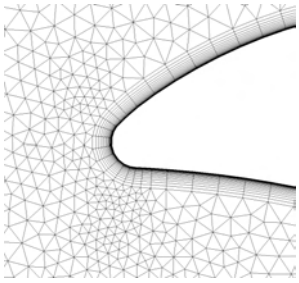

(b) Mesh 1, leading edge

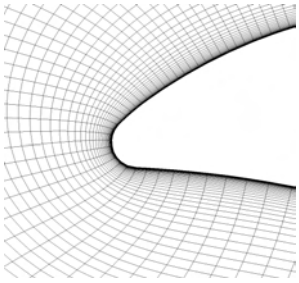

(c) Mesh 2, leading edge

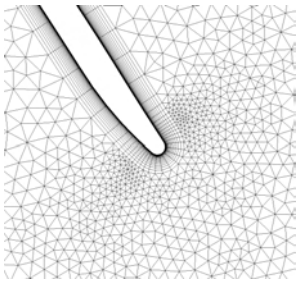

(d) Mesh 1, trailing edge

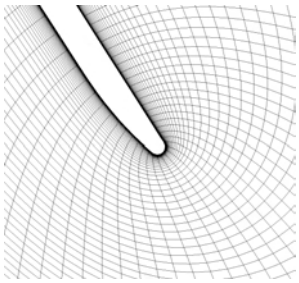

(e) Mesh 2, trailing edge

Figure 5: Computational meshes in the symmetry plane.

The second case models the non-uniform velocity profile formed in the inlet channel of the high speed wind tunnel. The measured total pressure $p_{1t}(z)$ was approximated assuming the power profile for the Mach number $M_1(z) \approx z^{1/7}$ leading to the functional form

$$p_{1t}(z) = p_{ref} \left[\frac{1 + \frac{\kappa-1}{2} M_1(z)^2}{1 + \frac{\kappa-1}{2} M_{ref}^2} \right]^{\frac{\kappa}{\kappa-1}}, \tag{7}$$

where $M_{ref} = 0.35$, $M_1(z) = M_{ref} \min(z/\delta, 1)^{1/7}$, $p_{ref} = 1.0 \times 10^5$ Pa, and δ is the inlet boundary layer thickness (see Fig. 4 for the case with $\delta = 30$ mm). The Reynolds number was $Re = 1.5 \times 10^6$.

The 3D calculation has been carried out using an unstructured mesh with 3.3×10^6 prismatic/hexahedral cells with mesh refinement in the vicinity of walls giving mesh with first cell bellow $y_1^+ < 1$ (mesh 1). In order to evaluate the mesh dependency of the results another calculation has been made with a structured multi-block mesh with 900×10^3 hexahedral cells (mesh 2). The figure 5 shows the unstructured and the multi-block meshes (denoted by mesh 1 and mesh 2) in the vicinity of leading and trailing edges.

3.1. Numerical results

The figure 6 shows the isolines of the Mach number in the symmetry plane ($z = 80$ mm) obtained with OpenFOAM using two above mentioned meshes and the Mach numbers obtained from 2D simulations carried out by the in-house solver using a mesh corresponding to mesh 1 and a mesh with refinement in the wake region. One can see that the OpenFOAM package (using mesh 1) gives similar results as the state-of art AUSM based scheme. The results obtained with mesh 2 shows correct position of the shock waves, nevertheless the shock waves are smeared much more than with the mesh 1.

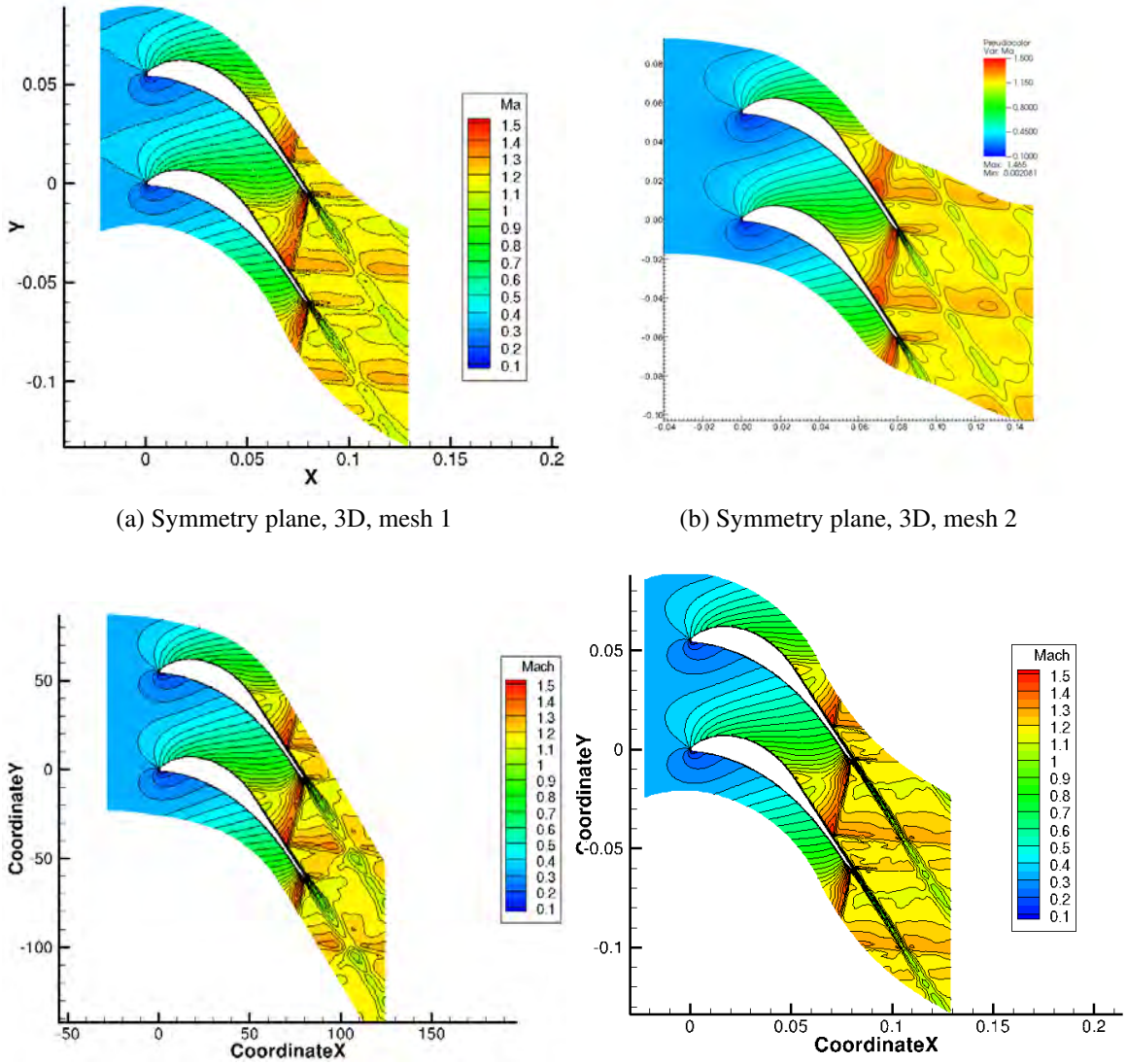

(a) Symmetry plane, 3D, mesh 1

(b) Symmetry plane, 3D, mesh 2

(c) 2D simulation

(d) 2D simulation, refined mesh

Figure 6: The Mach number in the symmetry plane compared to 2D results obtained with in-house solver.

4. The distribution of energy losses

The figure 7 shows the sketch of the traversing plane ($z = 110\,\text{mm}$) with the distribution of kinetic loss coefficieant defined as $\zeta = 1 - \lambda_2^2/\lambda_{2iz}^2$ where λ is the velocity magnitude related to the critical sound speed. The figure clearly shows that the losses are concentrated near the side walls and in the wake. The distribution of the losses is non-trivial. There is a local maximum in certain distance from the side wall caused by secondary flows.

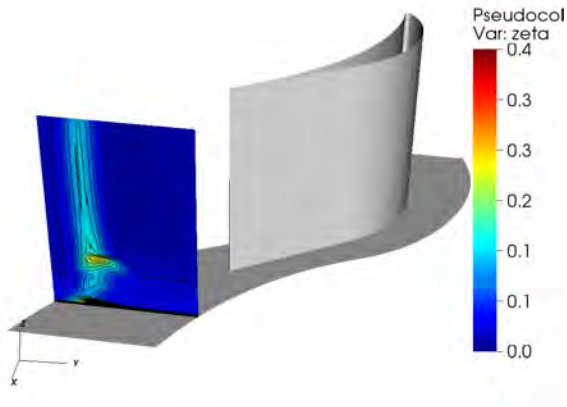

Figure 7: The distribution of kinetic energy losses ζ in traversing plane ($\delta = 30\,\text{mm}$).

The figure 8 compares the distribution of the energy losses obtained experimentaly at the Institute of Termomechanics with the numerical simulation with inlet boundary thickness $\delta = 30\,\text{mm}$. The numerical results are plotted for two periods with symmetry around channel midplane. The setup of the experiment didn't allow to measure the flow field close the side wall. Therefore the experimental data spans $10\,\text{mm} \leq z \leq 150\,\text{mm}$ whereas the numerical simulation is displayed in whole channel width. Although there are some quantitative differences in the loss coefficient, the position of local etrema obtained by the numerical simulation corresponds well with the experimental data ($z_{max} \approx 20\,\text{mm}$).

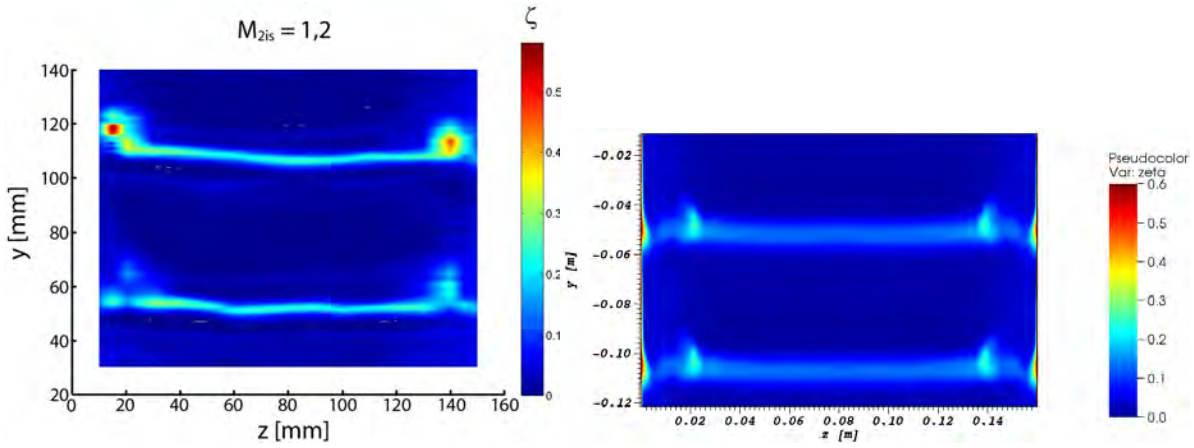

(a) Experiment, IT AS CR

(b) Numerical simulation

Figure 8: The distribution of loss coefficient ζ in the traversing plane ($M_2 = 1.2$, $\delta = 30\,\text{mm}$).

The figure 9 shows the distribution of pitch-wise averaged loss coefficient as a function of span-wise coordinate z. The comparison with experiment clearly documents that the calculation without considering non-uniform inlet velocity profile (denoted as $p_{t1} = const.$ in the figure) strongly under-estimates the losses in the near wall region. The position local extrema ($z_{max} \approx 9\,\text{mm}$) is wrong too. On the other hand considering the non-uniform inlet the calculation gives results which are closer to experimental data. One can see that the numerical simulation with $k - \omega$ SST model gives slightly higher losses in the middle of the channel whereas the losses in

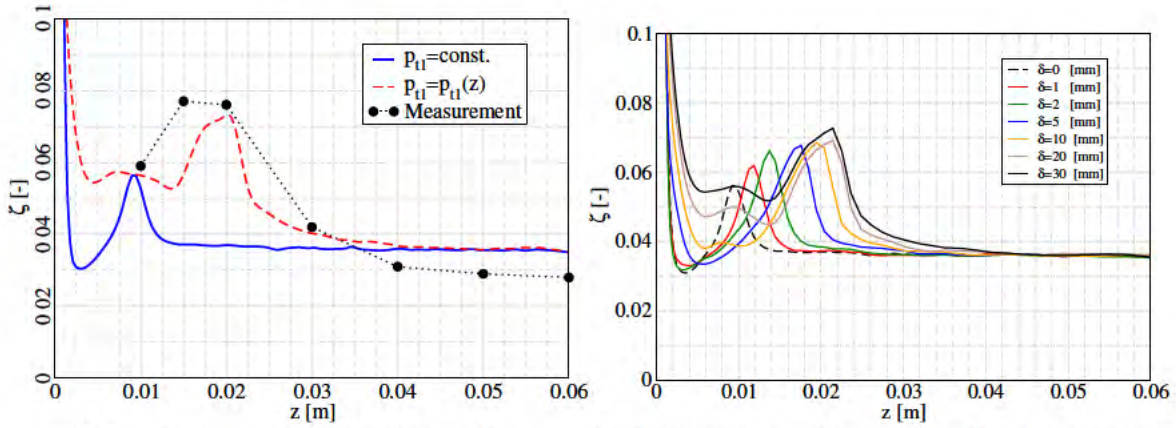

(a) Comparison with experiment ($\delta = 30$ mm)

(b) Distribution of ζ for different inlet boundary layer thickness.

Figure 9: The span-wise distribution of loss coefficient ζ.

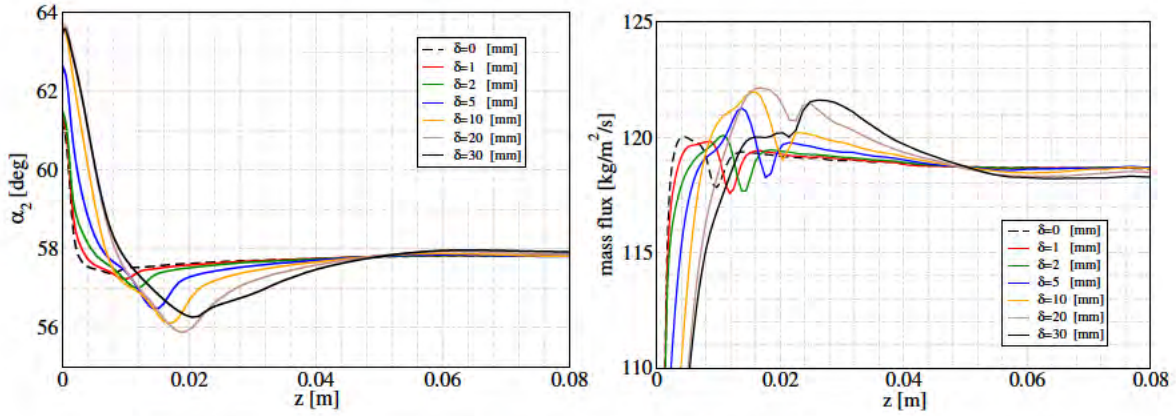

Figure 10: The span-wise distribution of pitch angle α_2 and mass flux.

the near-wall region are lower than the experimental data.

The figure 10 shows the distribution of the pitch-averaged outlet angle $\alpha_2(z)$ and of the mass flux. Both figures indicate that the flow field is influenced by the end-wall flows up to $z = 60$ mm (i.e. 3/4 of the channel width). The flow undergoes over-turning by 4° to 6° close to the side-wall followed by under-turning by 0° to 2° at the side-wall distance approximately corresponding to the position of maximal loses.

5. Conclusion

The span-wise distribution of the energy losses was studied for the case of prismatic turbine cascade in the transonic regime. Numerical simulations with different inlet boundary thickness demonstrate the dependency of the results on the inlet velocity profile. The consequence is that the detailed knowledge of the flow field in the inlet part of the wind tunnel is very important for numerical simulation of secondary flows in turbine cascade.

The comparison of numerical simulation with experimental data shows that the CFD simulation is capable of qualitatively resolve basic 3D flow effects. In accordance with findings made by Lampart (2009a), the numerical simulation overpredict the level of energy losses in

the wake in the middle part of the channel. This can be caused by the fact that the current turbulence model doesn't account for laminar-turbulent transition whereas the real flow is probably laminar at certain part of the blade, see e.g. Straka and Příhoda (2010). On the other hand the level of losses in near-wall flow is under-predicted with respect to the experiment which is in contrary with results of Lampart (2009a) obtained for subsonic flows.

6. Acknowledgment

The work was supported by the Grant no. P101/10/1329 of the Grant Agency of Czech Republic.

References

Ferziger, J. H. and M. Peric (1999). *Computational Methods for Fluid Dynamics*. Springer.

Fürst, Jiří (2006). "A Weighted Least Square scheme for Compressible Flows". In: *Flow, Turbulence and Combustion* 76.4, pp. 331–342. ISSN: 1386-6184.

Kozel, K. and J. Příhoda (2004). *ERCOFTAC QNET-CFD*. URL: `http://qnet-ercoftac.cfms.org.uk/w/index.php/Silver:AC_6-12_Description`.

Lampart, P. (2009a). "Investigation of Endwall Flows and Losses in Axial Turbines. Part I. Formation of Endwall Flows and Losses". In: *J. of Theoretical and Applied Mechanics* 47.2, pp. 321–342.

– (2009b). "Investigation of Endwall Flows and Losses in Axial Turbines. Part II. The Effect of Geometrical and Flow Parameters". In: *J. of Theoretical and Applied Mechanics* 47.4, pp. 829–853.

Luxa, Martin et al. (2012). "Causes and solution of aperiodicity of supersonic flow field downstream of a profile cascade". In: *Communications* 14/4a, pp. 23–28. ISSN: 1335-4205.

Matějka, M. et al. (2010). "Loss Coefficient Dependence of Turbine Blade Cascade". In: *ASME Paper* GT2010-22740.

Menter, F. R. (1994). "Two-Equation Eddy-Viscosity Turbulence Models for Engeenering Applications". In: *AIAA J.* 8.32, pp. 1598–1605.

Sieverding, C. H. (1985). "Recent Progress in the Understanding of Basic Aspects of Secondary Flows in Turbine Blade Passages". In: *ASME J. Turbomach.* 107, pp. 249–257.

Straka, P. and J. Příhoda (2010). "Application of the algebraic bypass-transition model for internal and external flows". In: *Proc Conf. Experimental Fluid Mechanics (EFM10)*. TU Liberec, pp. 636–641.

Šťastný, M. and P. Šafařík (1990). "Experimental Analysis Data on the Transsonic Flow Past the Plain Turbine Cascade". In: *ASME Paper* 90-GT-313.